UNIWERSYTET
WARMIŃSKO-MAZURSKI
W OLSZTYNIE

FLUID FLOW IN THE IMPULSE VALVE OF A HYDRAULIC RAM

Wojciech Sobieski, Dariusz Grygo

Faculty of Technical Sciences
University of Warmia and Mazury in Olsztyn, Poland

Abstract

The paper presents the results of a study investigating the equilibrium of forces acting on the closing element of the impulse valve in a water ram at the end of the acceleration stage. Acceleration is one of the three main stages in the working cycle of a water ram. In the first part of the paper, we estimated water velocity based on our earlier experimental measurements. We also calculated the minimum force required for closing the impulse valve. The second part of the paper discusses two variants of a numerical model, which was developed in ANSYS Fluent to determine the resultant hydrodynamic pressure and, consequently, the forces acting on the head of the impulse valve at the end of the acceleration stage. The main aim of this research was to verify the applicability of numerical modeling in water ram studies. The present study was motivated by the fact that Computational Fluid Dynamics is very rarely applied to water rams. In particular, we have not found any numerical studies related to the equilibrium of forces acting on the closing element of the impulse valve in a water ram.

Introduction

A water ram is a pump which lifts water by relying on the energy of water flow. The pump can be supplied from any hydraulic source with a sufficient amount of water to guarantee a working fall. The minimum water head is approximately 1 m

Correspondence: Wojciech Sobieski, Katedra Mechaniki i Podstaw Konstrukcji Maszyn, Wydział Nauk Technicznych, Uniwersytet Warmińsko-Mazurski, ul. M. Oczapowskiego 11, 10-957 Olsztyn, phone +48 (89) 523 32 40, e-mail: wojciech.sobieski@uwm.edu.pl; ORCID: 0000--0003-1434-5520.

(MOHAMMED 2007, WATT 1975). This requirement has to be met to overcome friction forces (caused by water viscosity and turbulence), increase the flow rate of supply water and produce sufficiently large forces in the system.

Water flows freely through the working zone (zone *A*) of a water ram at the beginning of the cycle. The closing element (*4*) of the impulse valve (*3*) is in the down (open) position (Fig. 1). Water flows through an open impulse valve (*3*) and outside the ram pump into an evacuation channel or is indirectly fed to the source which supplies the ram. The Earth's gravity speeds up the flow of water in the working zone, thus increasing the hydrodynamic force acting on the closing element of the impulse valve (*4*). When the appropriate flow rate has been achieved, the hydrodynamic force exerted by water on the closing element of the impulse valve increases substantially and finally closes the valve (*Hydraulic ram pumps* 2019, *Water-powered* water… 2019, Meribah Ram Pump 2019, SHEIKH et al. 2013). The sudden cessation of water flow in the working zone produces a positive water hammer (BERGANT et al. 2006, CHOON et al. 2012, GHIDAOUI et al. 2005). The maximum pressure during water hammer is several or more than ten times higher than in the preceding phase (CHOON et al. 2012, GHIDAOUI et al. 2005, LANDAU, LIFSZYC 2009). The increase in pressure is determined mainly by the flow rate in the drive pipe, the rate of change in flow velocity, the stiffness of pump and drive pipe materials, and the amount of air in water (GRYBOŚ 1998, NAŁĘCZ, PIETKIEWICZ 2000a, 2000b). The resulting shock wave opens the pressure valve (*5*), and a certain amount of water enters the pressure zone (zone *B*). The pressure in the pressure zone increases after start-up, and it reaches a much higher level than the average pressure in the working zone. Pressure in the pressure zone is determined by delivery head (h_c).
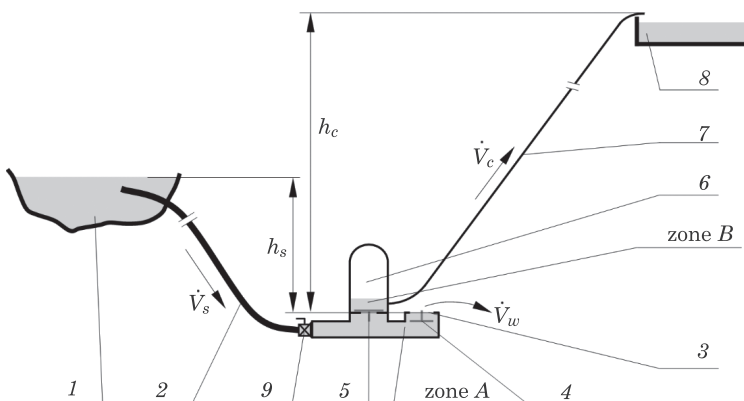
Fig. 1. Diagram of a water ram: *1* – water source, *2* – drive pipe, *3* – impulse valve, *4* – closing element of the impulse valve, *5* – pressure valve, *6* – air chamber, *7* – delivery pipe, *8* – water collector, *9* – shut-off valve, h_s – height of the water supply source, h_c – height of water outflow (delivery head), $\dot{V}_s$ – flow rate of water supply, $\dot{V}_c$ – rate of water outflow to the water collector, $\dot{V}_w$ – rate of water outflow to the surrounding environment; zone *A* – working zone, zone *B* – pressure zone; the impulse valve and the check valve are one-way (non-return) valves

The air chamber (*6*) in the pressure zone minimizes pressure fluctuations in the delivery system. The movement of water from zone *A* to zone *B* (upwards) does not last long because the system is not in equilibrium, and flow quickly subsides in the delivery pipe. The movement of water is suppressed by the gravitational force, and water begins to flow downwards in the direction of the water source supplying the ram. The closing element of the pressure valve is moved by flowing water, and the pressure valve is closed. The closure of the pressure valve in the working zone produces negative water hammer, which opens the impulse valve and marks the beginning of a new cycle in a water ram.

This article presents selected aspects of an extensive research study analyzing the processes that occur in a single water ram cycle (GRYGO 2018, GRYGO, SOBIESKI 2015a, 2015b, SOBIESKI et al. 2016). The efficiency of water rams was tested in various configurations. The results were processed statistically, and the identified relationships were presented as regression equations (GRYGO 2018). The present study relied on data from the main stage of experimental measurements. The analyzed configuration has been described previously in (SOBIESKI et al. 2016).

In this study, the Finite Volume Method was used to simulate the operation of a water ram in the acceleration stage (water flows through the impulse valve only in the acceleration stage) based on geometry and flow rates in the experimental test rig. It should also be noted that numerical investigations of water rams have been rarely described in the literature. One of such studies was conducted by HARITH et al. (2017), but we cannot directly refer to their findings due to different research objectives and water ram constructions. Maw and HTET (2014) performed a simple analysis of pressure and velocity distribution in a water ram with the use of Solid Work software, but they did not discuss the equilibrium of the impulse valve. A similar study, performed using the Fluent code, was presented by SHENDE et al. (2015). However, the scientific merit of this study is relatively since the authors reported numerous results followed by a very brief (2-page) discussion. VERSPUY and TIJSSELING (1993) described the operation of a water ram, but they did not use the tools of Computational Fluid Dynamics (CFD) and instead relied on an analytical model based on the standard water hammer theory. Yet another model was presented by TIJSSELING and BERGANT (2012). However, the authors did not focus on water rams but on water hammer phenomena in a system of three connected reservoirs. One of the most advanced models was described by FILIPAN et al. (2003) who, however, used self-developed software instead of CFD tools.

Test stand

The test stand was composed of (Fig. 2): ¾ in drive pipe with the length of 7 m (*1*); ½ in delivery pipe (*2*); a welded ½ in steel pipe which constitutes the body of the water ram (*3*); air chamber (*4*) made of a PE pipe with a diam-

eter of 65 mm, wall thickness of 4 mm and chamber volume of 1 dm^3, closed with plugs (*5*); one-way brass ½ in impulse valve (*6*) without spring retainers; one-way brass ½ in valve (*7*); connectors (*8*) for electronic pressure transducers (*9*); ball valve (*10*) for starting up the water ram; ball valve (*11*) for cutting off the delivery pipe; ball valve (*12*) for evacuating water from the delivery pipe.
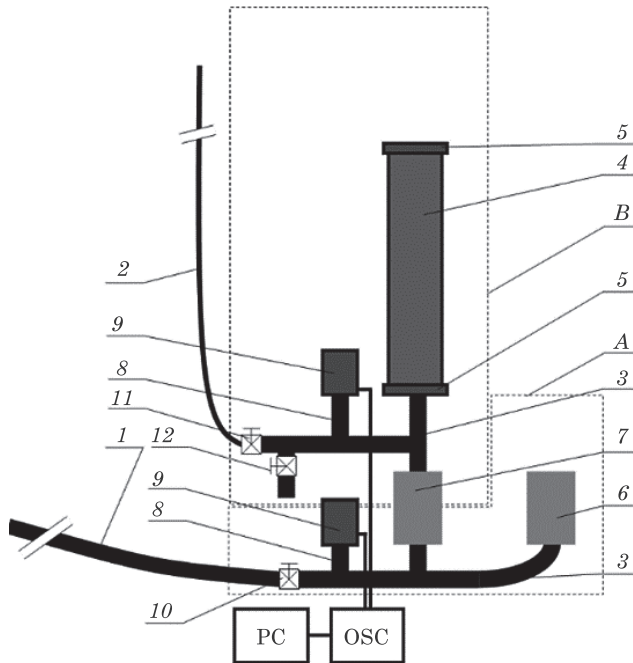
Fig. 2. Diagram of the experimental installation

The water ram was shut off for more than ten minutes before the measurements. Water head in the supply source and the height of the water tank were determined with a laser level and measuring tape. The experiment was conducted in a system with $h_s = 4.96$ m and $h_c = 16$ m. The pressure measurement system was checked. Changes in pressure were recorded with the EZ Digital DS-1080C laboratory oscilloscope with 80 MHz bandwidth and 100 MSa/s sample rate per channel, and Wika Model A-10 electronic pressure transducers. The time base was set at 0.02 to 0.1 s, and sensitivity – at 0.2 to 2 V.

Analysis of experimental data

The experimental stage has been described in detail by (SOBIESKI et al. 2016) and (GRYGO 2018). In this section, we estimated water velocity at the end of the acceleration stage needed to defining the boundary conditions in the numerical model. We also calculated the minimum force required for closing the impulse valve.

Changes in pressure in two zones of the water ram during a single working cycle are presented in Figure 3. The top line (denoted by number 1) represents changes in pressure in the working zone (*A*), and the bottom line (denoted by number 2) represents changes in pressure in the pressure zone (*B*). The duration of a single water ram cycle and the acceleration stage is indicated in the diagram.
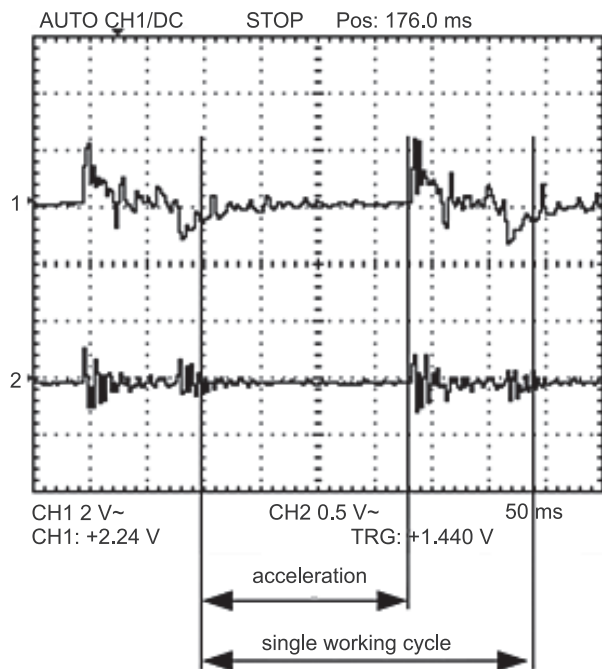
Fig. 3. Changes in pressure during a single working cycle of a water ram

The results of the experimental measurements indicate that 14 dm^3 of water flowed through the impulse valve and that the water ram completed 617.4 cycles in 3 minutes on average. TACKE (1998) reported that depending on supply head, waste valve adjustment and, to a lesser degree, on drive pipe length and delivery head, the cycle is repeated with a frequency of around 30 to 150 times per minute.

In our study, the above frequency was higher due to the fact that TACKE (1998) used massive industrial water rams whereas we used a small pump composed of typical hydraulic components. Another reason could be that the ratio between the height of the water supply source and the length of the delivery pipe was relatively small. However, the relevant data were not available and we could not evaluate the impact of this ratio on the operation of the water ram. Effective flow rate was determined at 0.00007777 m^3/s. Effective flow rate is the flow rate determined based on the total time of the measurement. The actual flow rate is higher because the acceleration stage is shorter than a single working cycle (207 ms) (SOBIESKI et al. 2016). Therefore, when the impulse valve is open, flow rate over time should be calculated with the use of the below formula:

$$\dot{V}_a = \frac{V}{t \cdot X_a} \tag{1}$$

where:
$\dot{V}_a$ – volumetric flow rate in the impulse valve in the acceleration stage [m^3/s],
V – volume of water flowing through the impulse valve during the measurement [m^3],
t – duration of measurement [s],
X_a – ratio of the duration of the acceleration stage to the duration of a single working cycle (0.7055 in the analyzed case).
For the measured data, $\dot{V}_a = 0.00010954$ m^3/s.

The average water velocity in the acceleration stage can be calculated based on the internal diameter of the impulse valve equal to 0.012 m.

$$c_a = \frac{4 \cdot \dot{V}_a}{\pi \cdot d^2} \tag{2}$$

The result is 0.873 m/s for the measured data.
The scenario described by formula (2) is presented graphically in Figure 4a. In this variant, the water flow rate is assumed to be constant when the impulse valve is open. In reality, the initial flow rate is zero, and it begins to increase gradually when the impulse valve is opened (acceleration stage). However, the exact nature of the observed changes could not be described due to the complex internal geometry of the impulse valve. The conducted measurements revealed that the water flow rate increases over time. The above is presented in Figure 4b on the assumption that water velocity increases in a linear fashion. To obtain the same flow rate for the same period of time:

$$\dot{V}_a = \int_0^{t_a} \dot{V}_1(t)\mathrm{d}t = \int_0^{t_a} \dot{V}_2(t)\mathrm{d}t \tag{3}$$

the maximum velocity has to be twice that calculated for the previous variant.
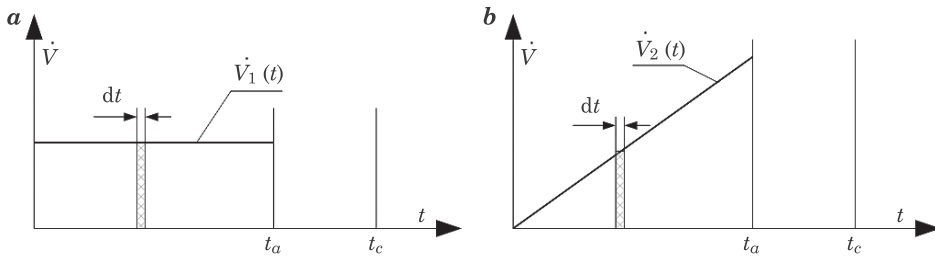
Fig. 4. Changes in flow rate over time: constant value (*a*) and increase (*b*)

Therefore:

$$c_{a,\max} = 2 \cdot c_a \tag{4}$$

where: $c_{a,\max}$ is the maximum velocity in the acceleration stage. This parameter was determined at 1.746 m/s for the measured values.

An analysis of the forces acting on the closing element of the impulse valve suggests that changes in valve position can be expressed as follows (*ANSYS Fluent in ANSYS…* 2012):

$$\vec{F}_a = \vec{a} \cdot \vec{F}_p + \vec{a} \cdot \vec{F}_v > \vec{G} \tag{5}$$

where:

$\vec{F}_a$ – resultant force in a given direction [N],
$\vec{a}$ – direction vector [–],
$\vec{F}_p$ – normal force (pressure) vector [N],
$\vec{F}_v$ – contact force (friction) vector [N],
$\vec{G}$ – weight force of the closing element of the impulse valve [N].

The closing element of the impulse valve applied in the experiment had a mass of 37.75 g, which is equivalent to the weight of 0.3703 N.

Numerical model

The Finite Volume Method was applied in numerical investigations. In this method, two main types of balance can be identified, namely surface balance and volumetric balance. The surface balance describes the possibility of exchanging a given physical quantity between the system and the surroundings via fluxes flowing through the surface of a Finite Volume. The volumetric balance describes the possibility of changing the balanced physical quantity within a Finite Volume.

The main set of balance equations may have the following form (SOBIESKI 2011):

$$\begin{cases} \dfrac{\partial \rho}{\partial t} + \mathrm{div}(\rho \vec{v}) = 0 \\[2mm] \dfrac{\partial (\rho \vec{v})}{\partial t} + \mathrm{div}\big(\rho \vec{v}\vec{v} + p\overleftrightarrow{I}\big) = \mathrm{div}(\overleftrightarrow{\tau}^{m} + \overleftrightarrow{\tau}^{R}) + \rho s_b \\[2mm] \dfrac{\partial (\rho e)}{\partial t} + \mathrm{div}\big(\rho e \vec{v} + p\overleftrightarrow{I}\vec{v}\big) = \mathrm{div}[(\overleftrightarrow{\tau}^{m} + \overleftrightarrow{\tau}^{R})\vec{v} + \vec{q}^{m} + \vec{q}^{R}] + \rho s_e \end{cases} \tag{6}$$

where:

ρ – density [kg/m^3],
$\vec{v}$ – velocity [m/s],
p – static pressure [Pa],
$\overleftrightarrow{I}$ – unit tensor [–],
$\overleftrightarrow{\tau}^{m}$ – viscous molecular stress tensor [Pa],
$\overleftrightarrow{\tau}^{R}$ – turbulent Reynolds stress tensor [Pa],
s_b – source of unitary mass forces [N/kg],
e – sum of kinetic and internal energy [N/(kg s)],
$\vec{q}^{m}$ – molecular heat flux [J/(m^2·s)],
$\vec{q}^{R}$ – turbulent heat flux [J/(m^2·s)],
s_e – sources of heat [J/(m^3·s)].

The set of balance (or transport) equations (6) is not complied and needs to be supplemented by many "closures", which means that specific models describe individual problems (SOBIESKI 2013).

To develop a model simulating water flow through the impulse valve, the geometry of computational space has to be defined, a numerical grid has to be generated, boundary and initial conditions have to be defined, and the appropriate methods for solving numerical problems have to be selected.

The impulse valve was removed and disassembled to collect information about system geometry. All parts and dimensions were measured with an electronic caliper with a rated accuracy of 0.02 mm. System geometry and the numerical grid representing areas of water flow inside the valve are presented in Figure 5. The model was developed in the ANSYS v. 14.5 package (*Design Modeler User's Guide...* 2012, *ANSYS Fluent Meshing...* 2012, *ANSYS Fluent User's Guide...* 2012). All components of the closing element of the impulse valve (marked with different colors in Figure 5*a*) were grouped and given a collective name. This approach facilitated the calculation of the resultant normal and contact forces acting on all components of the closing element. It should also be noted that the valve's axis of symmetry was aligned with the *Y*-axis in the adopted system of coordinates. The rotation of the axis of symmetry denotes the direction of water flow (this axis is not presented in Figure 5, but it is shown in successive figures).
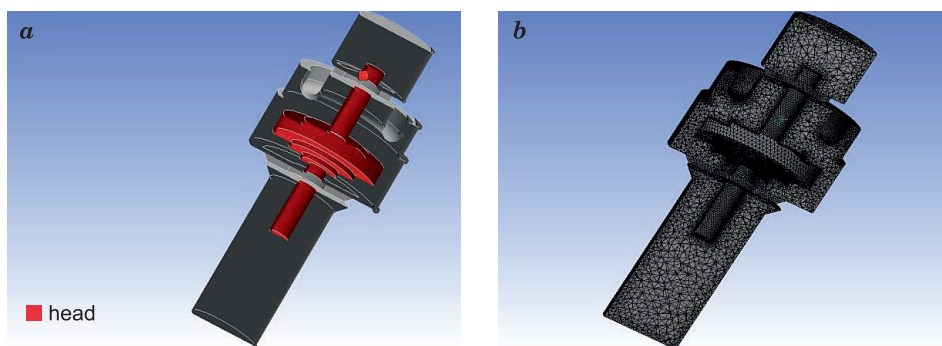
Fig. 5. Area of water flow inside the impulse valve: geometry (*a*) and the numerical grid (*b*)

The boundary and initial conditions of the numerical model were defined based on the experimentally measured values, and two variants were analyzed. The first variant involves a velocity inlet (boundary condition based on velocity; pressure is calculated during the simulation), and the second variant involves a pressure inlet (boundary condition based on pressure; velocity is calculated during the simulation). In the first variant, inlet velocity was the maximum velocity calculated with formula (4). This approach was adopted to analyze the situation in the system at the end of the acceleration stage. In the second variant, total pressure (p_t) was total static pressure resulting from water head in the supply source and dynamic pressure calculated for the maximum velocity:

$$p_t = \rho \cdot g \cdot h_s + \frac{\rho \cdot c_{a,\max}^2}{2} \qquad (7)$$

which produces 50,138 Pa for the experimental values (dynamic pressure equals 1,523 Pa). In both variants, the pressure boundary condition at the inlet was equal to 101,325 Pa.

The parameters of the simulation model are presented in Table 1. All settings that did not result directly from the experimental data were assigned default values (*Theory Guide. Release 14.5.* 2012, *Tutorial Guide. Release 14.5.* 2012). This approach is recommended for modeling the flow of single-component fluids. Default values were also applied because turbulence parameters were unknown. The relevant measurements could not be performed during the experiment.

The distribution of total pressure on the closing element of the impulse valve in both variants is presented in Figure 6. The closing element is symmetrical, but four areas of higher pressure can be identified. The above can be attributed to the presence of guides that control the closing elements of the impulse valve. The guides separate the water stream in the top segment and cause macro-turbulence and micro-turbulence. Local pressure drops occur behind the guides, and the pressure on the closing element is highest in areas where water flow is unobstructed.

Parameters of the simulation model

No.	Parameter	Variant 1	Variant 2
1	Solver type	pressure based	
2	Velocity formulation	absolute	
3	Time	steady	
4	Gravity	-9.81 m/s^2 (in relation to *Y*-axis)	
5	Energy equation	off	
6	Viscous model	*k-ε* standard with standard wall function	
7	Water density	999.13 kg/m^3	
8	Viscosity	0.001003 kg/m·s	
9	Inlet velocity	1.746 m/s	-
10	Inlet initial gauge pressure	-	50,138 Pa
11	Inlet dynamic pressure	-	1,523 Pa
12	Turbulent intensity	5%	
13	Turbulent Viscosity Ratio	10	
14	Outlet pressure	101,325 Pa	
15	Turbulent intensity	5%	
16	Turbulent Viscosity Ratio	10	

Fluid velocity increases in valve grooves (Fig. 7). Local velocity is much higher than the average velocity calculated in the previous section. The option of calculating complete pressure and velocity fields is an unquestioned advantage of numerical modeling, and these values cannot be derived with the use of analytical methods. It should also be noted that the method of defining the inlet significantly influences fluid velocity in the entire computational area, and higher values were noted in variant 2.

Path lines colored according to static pressure are presented in Figure 8.

Static pressure is calculated relative to the reference value of 101,325 Pa. Static pressure decreased in the valve from around 31,100 Pa (variant 1) or 50,100 Pa (variant 2) to around zero, i.e. to the reference value (atmospheric pressure). Minor areas of negative pressure can be observed locally behind flow obstructions. These areas are not presented in the figures, but they can be deduced from the range of values in the legend.

An analysis of pressure and velocity values in the computational area indicates that velocity is adequate in variant 1 (velocity was input directly), whereas pressure in the top segment is too low. In variant 2, pressure is adequate (pressure was input directly), whereas velocity appears to be too high. Based on the experimental data, variant 1 seems to be a better option.

After numerical simulations, the resultant force acting on the closing element of the impulse valve in the direction of the Y-axis was calculated (the appropriate tool can be found in ANSYS Fluent). Under the simulated conditions, the resultant force was determined at 0.79 N in variant 1 and 1.32 N in variant 2. The resultant force is higher in variant 2 due to higher fluid velocity than in variant 1.
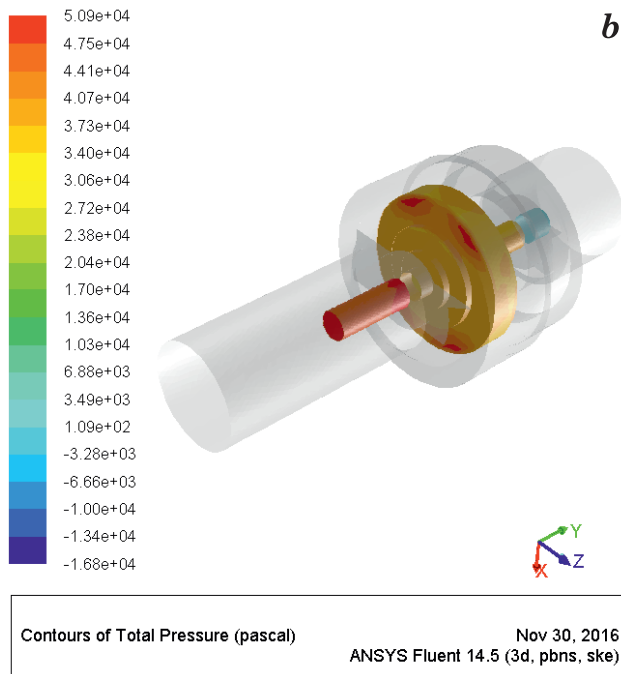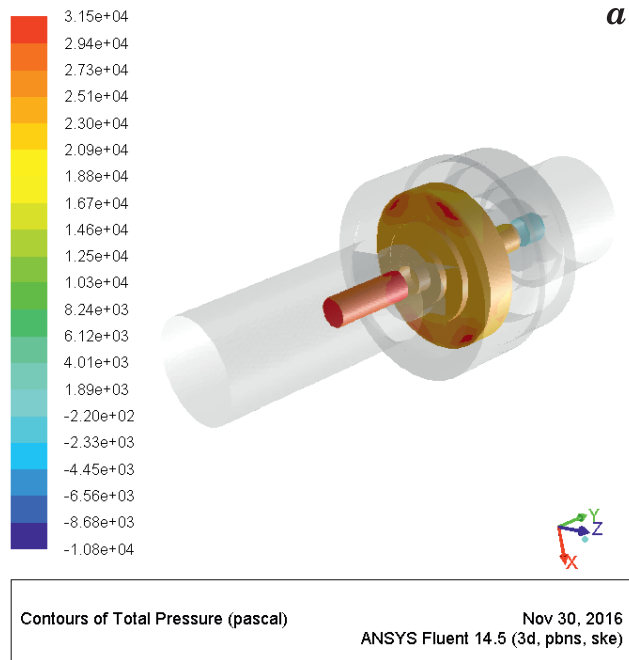
Fig. 6. Distribution of total pressure on the head of the impulse valve
in variant 1 (*a*) and variant 2 (*b*)
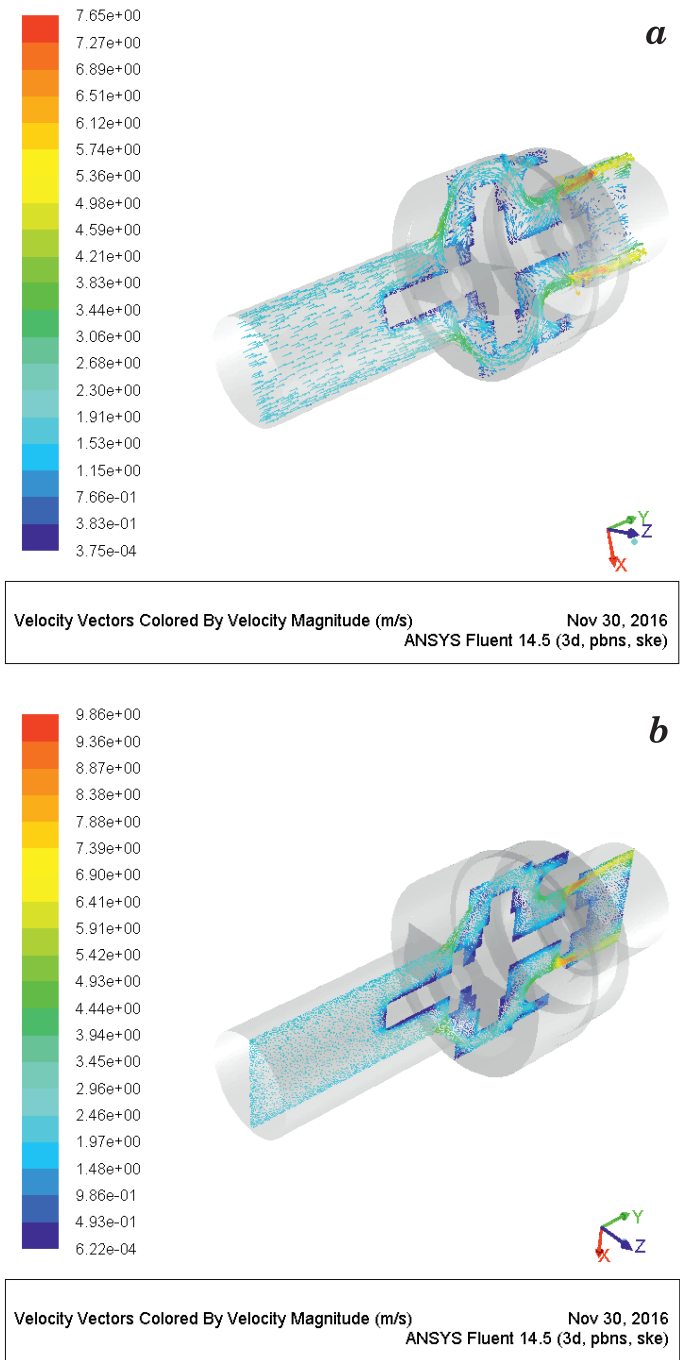
Fig. 7. Velocity fields for selected longitudinal cross-sections of the impulse valve
in variant 1 (*a*) and variant 2 (*b*)
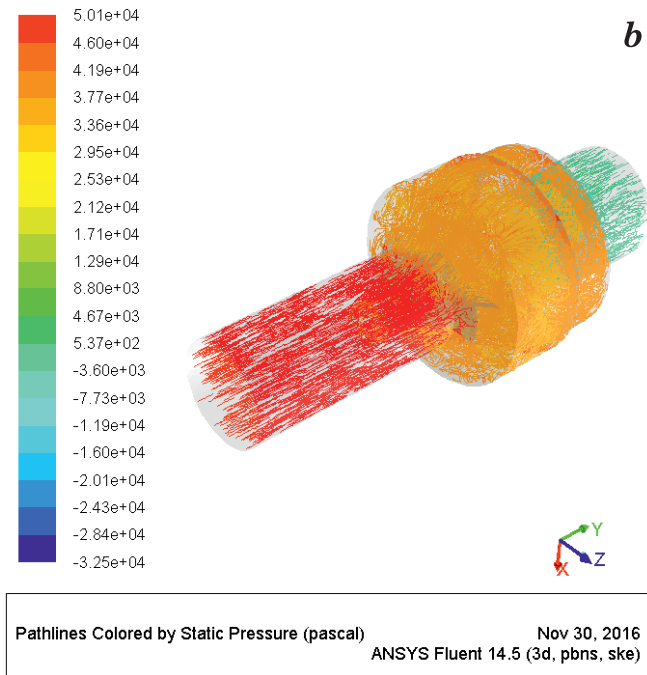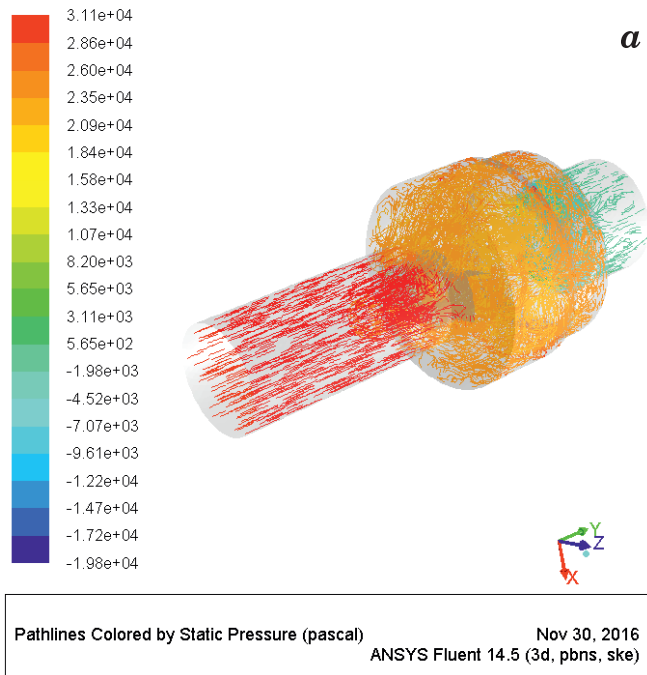
Fig. 8. Path lines colored according to pressure in variant 1 (*a*) and variant 2 (*b*)

The calculated interaction forces exceeded the weight of the impulse valve head 2.13-fold (variant 1) and 3.55-fold (variant 2). The above implies that the balance of forces at time t_a should be sufficient to close the valve. It should also be noted that time t_a marks the end of the acceleration stage which, as described in a previous study (SOBIESKI et al. 2016), is composed of three phases during which the impulse valve begins to open, the impulse valve is open, and the impulse valve begins to close. Therefore, interaction forces and the weight of the valve head were equalized earlier, i.e. before time t_a.

Summary

The following conclusions can be formulated based on the results of the present study:

• Numerical tools for fluid mechanics can be used to calculate the forces acting on selected elements that obstruct fluid flow, including the closing element of the impulse valve in a water ram pump. These tools can be applied to design new types of impulse valves that close faster (have a lower value of coefficient X_a) and, consequently, increase system efficiency.

• Numerical simulations produce higher values of interaction forces between flowing water and the closing element of the impulse valve than simple estimations (whose reliability is limited due to oversimplification). However, the degree of consistency between the simulation model and the experimental data is difficult to assess because in a real-world system, the closing element of the impulse valve begins to close before time t_a, and water flowing during valve closure can still accelerate and increase the force acting on the closing element of the impulse valve.

• The experimental data indicate that average fluid velocity (which is a key parameter in the defined model) should be calculated and that a velocity inlet should be incorporated in the numerical model.

• The scope of numerical analyses should be expanded in the future by evaluating the impact of the adopted turbulence model (and its parameters) on pressure values.

REFERENCES

ANSYS Fluent in ANSYS Workbench User's Guide. Release 14.5. 2012. ANSYS Inc.

ANSYS Fluent Meshing User's Guide. Release 14.5. 2012. ANSYS Inc.

ANSYS Fluent User's Guide. Release 14.5. 2012. ANSYS Inc.

BERGANT A., SIMPSON A.R., TIJSSELING A.S. 2006. *Water hammer with column separation: A historical review*. Journal of Fluids and Structures, 22: 135-171.

CHOON T.W., AIK L.K., AIK L.E., HIM T.T. 2012. *Investigation of Water Hammer Effect Through Pipeline System*. International Journal on Advanced Science Engineering Informational Technology, 2(3): 48-53.

Design Modeler User's Guide. Release 14.5. 2012. ANSYS Inc.

FILIPAN V., VIRAG Z., BERGANT A. 2003. *Mathematical modelling of a hydraulic ram pump system.* Journal of Mechanical Engineering (Strojniški vestnik), 49(3): 137-149.

GHIDAOUI M.S., ZHAO M., McINNIS D.A., AXWORTHY D.H. 2005. *A Review of Water Hammer Theory and Practice.* Applied Mechanics Reviews, 58: 49-76.

GRYBOŚ R. 1998. *Fundamentals of fluid mechanics.* PWN, Warszawa.

GRYGO D. 2018. *Analysis of the phenomena occurring during the water ram operation.* PhD Thesis, University of Warmia and Mazury in Olsztyn, The Faculty of Technical Sciences, Olsztyn.

GRYGO D., SOBIESKI W. 2015a. *Position of laboratory to phenomena research running in the ram water.* Mechanik, 7: 237-244.

GRYGO D., SOBIESKI W. 2015b. *Proposals to use hydraulic rams.* Woda-Środowisko-Obszary Wiejskie, 15: 31-47.

HARITH M.N., BAKAR R.A., RAMASAMY D., QUANJIN M. 2017. *A significant effect on flow analysis & simulation study of improve design hydraulic pump.* 4th International Conference on Mechanical Engineering Research (ICMER 2017). doi:10.1088/1757-899X/257/1/012076.

Hydraulic ram pumps. 2019. Appropedia. http://www.appropedia.org/Hydraulic_ram_pumps (February 28, 2019).

LANDAU L., LIFSZYC J. 2009. *Hydrodynamics.* PWN, Warszawa.

MAW Y.Y., HTET Z.M. 2014. *Design of 15 meter Head Hydraulic Ram Pump.* International Journal of Scientific Engineering and Technology Research, 3(10): 2177-2181.

MOHAMMED S.N. 2007. *Design and Construction of a Hydraulic Ram Pump.* Leonardo Electronic Journal of Practices and Technologies. 11: 59-70.

NAŁĘCZ T., PIETKIEWICZ P. 2000a. *Influence of air as the second phase for the velocity propagation of shock wave into multilayer pipe.* XVIII Conference of Research, Design, Production and Operating of Hydraulic Systems, Cylinder, Szczyrk.

NAŁĘCZ T., PIETKIEWICZ P. 2000b. *Determining of the velocity of the propagation impact wave into hydraulic lines with taking into account air as second phase.* XII National Conference Pneuma, Kielce, p. 255-262.

SHEIKH S., HANDA C.C., NINAEW A.P. 2013. *Design methodology for hydraulic ram pump (hydram).* International Journal of Mechanical Engineering and Robotics Research, 2(4): 170-175.

SHENDE P. B., CHOUDHARY S.K., NINAWE A.P. 2015. *Analysis and Enhancement of Hydraulic Ram Pump using Computational Fluid Dynamics (CFD).* International Journal for Innovative Research in Science & Technology, 2(3): 2349-6010.

SOBIESKI W. 2011. *The basic equations of fluid mechanics in form characteristic of the finite volume method.* Technical Sciences, 14(2): 299-313.

SOBIESKI W. 2013. *The basic closures of fluid mechanics in form characteristic for the Finite Volume Method.* Technical Sciences, 16(2): 93-107.

SOBIESKI W., GRYGO D., LIPIŃSKI S. 2016. *Measurement and analysis of the water hammer in ram pump.* Sadhana, 41(11).

TACKE J.H.P.M. 1988. *Hydraulic rams − a comparative investigation.* Communications on Hydraulic and Geotechnical Engineering, Delft University of Technology, Faculty of Civil Engineering, Report 88-1, ISSN 0169-6548. http://repository.tudelft.nl/.

Theory Guide. Release 14.5. 2012. ANSYS Inc.

TIJSSELING A.S., BERGANT A. 2012. *Exact computation of waterhammer in a three-reservoir system.* CASA-Report 12-41, December 2012, Eindhoven University of Technology, The Netherlands.

Tutorial Guide. Release 14.5. 2012. ANSYS Inc.

VERSPUY C., TIJSSELING A.S. 1993. *Hydraulic ram analysis.* IAHR Journal of Hydraulic Research, 31: 267-278.

Water-powered water pumping systems for livestock watering. 2019. Canada Agriculture and Agri-Food. http://www1.agric.gov.ab.ca/$department/deptdocs.nsf/ba3468a2a8681f69872569d60073f-de1/42131e74693dcd01872572df00629626/$FILE/wpower.pdf (February 28, 2019).

WATT S.B. 1975. *A manual on the hydraulic ram for pumping water*. Intermediate Technology Development Group, Water Development Unit, National College of Agricultural Engineering, Bedford.
Why Meribah Ram Pump? 2019. Meribah Ram Pump. https://www.meribah-ram-pump.com/ (January 8, 2019).